Inverse Problems, Design and Optimization Symposium
Rio de Janeiro, Brazil, 2004

ITERATIVE IMAGE RECONSTRUCTION IN THREE-DIMENSIONAL ELECTRICAL IMPEDANCE TOMOGRAPHY

Päivi J. Vauhkonen
Marko Vauhkonen
Aku Seppänen
Jari P. Kaipio
Department of Applied Physics
University of Kuopio
Kuopio, Finland
Paivi.Vauhkonen@uku.fi

ABSTRACT

In this paper we consider iterative reconstruction in three-dimensional electrical impedance tomography (EIT). We propose a special block-nonlinear conjugate-gradient method for the reconstruction. The proposed method requires less storage in the computation, in comparison with the traditional methods. This feature is highly important in three-dimensional imaging where large-dimensional systems of equations are needed to be solved, The proposed method is tested with a computer simulation. The importance of inexact line search in the optimization is also studied numerically.

NOMENCLATURE

e_ℓ – ℓ'th electrode

F – Functional to be minimized

I_ℓ – electric current on $\ell^{\rm th}$ electrode

I – current pattern $I = (I_1, \ldots, I_L)$

J – Jacobian matrix $J = \frac{\partial U}{\partial \rho}(\rho_k)$

L – number of electrodes

L_2 – regularization matrix

n – outward unit normal

p_k – search direction in line search

$U = U(\rho)$ – mapping between resistivity ρ and the boundary voltages

u – potential distribution

V – voltage observations

v – additive gaussian noise

z_ℓ – contact impedance

α_k – step parameter in line search

β_k – step parameter for search direction

λ – regularization parameter

$\partial\Omega$ – boundary of domain Ω

ρ – resistivity distribution

ρ^* – prior guess for resistivity

σ – conductivity distribution

INTRODUCTION

EIT is an imaging modality used in medical, industrial and geological applications. In EIT electrical boundary measurements are used for reconstructing the three-dimensional resistivity distribution inside the target. Alternating currents are injected into the object through electrodes which are attached on the boundary. The resulting voltages are measured with the same electrodes, and the internal resistivity distribution is computed based on the voltage measurements. This estimation prob-

lem is a nonlinear and ill-posed inverse problem.

In some applications the two-dimensional models are adequate in EIT. However, in most cases the three-dimensional modeling is needed. The injected currents spread out in three dimensions, and if this is not taken into account in the models, off-plane structures may cause large errors in the reconstructions. Three-dimensional modeling, however, results in solving large-dimensional systems of equations; in realistic EIT problems, for example in head imaging, thousands of unknown resistivity parameters are to be determined. The computations take a lot of computer time and storage, and therefore the solution method plays a significant role. Because of the nonlinearity and ill-posedness of EIT standard optimization approaches can not be utilized.

In this paper a finite element-based method for the reconstruction of three-dimensional resistivity distributions is used. The proposed method is based on the so-called complete electrode model that takes into account the presence of the electrodes and the contact impedances. We have studied different types of iterative optimization methods for the solution of the inverse problem. A special nonlinear conjugate-gradient method for 3D EIT is proposed. The advantage of the conjugate-gradient methods is that the expense of inverting large dimensional matrices can be avoided. In addition, in the proposed block-nonlinear conjugate-gradient method the gradients needed for the search direction can be computed in separate blocks. This reduces further the need of storage in the computation and allows parallelization. The proposed approaches are tested with a computer simulation.

FORWARD MODEL

In EIT alternating currents I_ℓ are applied to electrodes on the surface of the object and the resulting voltages U_ℓ on these electrodes are measured. The resistivity distribution ρ is reconstructed based on the voltage measurements. In the case of additive noise the observation model of EIT is of the form

$$V = U(\rho) + v, \tag{1}$$

where V is a vector including the RMS-values of the measured voltages, U is a model between the resistivity ρ and the measurements, and v is additive observation noise.

The most accurate for EIT is called the complete electrode model [1,2]

$$\begin{aligned}
\nabla \cdot (\sigma \nabla u) &= 0\,, \quad x \in \Omega && (2)\\
u + z_\ell \sigma \frac{\partial u}{\partial n} &= U_\ell\,, x \in e_\ell,\ \ell = 1, ..., L && (3)\\
\int_{e_\ell} \sigma \frac{\partial u}{\partial n}\, dS &= I_\ell\,, x \in e_\ell,\ \ell = 1, ..., L && (4)\\
\sigma \frac{\partial u}{\partial n} &= 0\,,\ x \in \partial\Omega \backslash \bigcup_{\ell=1}^{L} e_\ell && (5)
\end{aligned}$$

where $\sigma = \rho^{-1}$ is the conductivity distribution, u is the scalar potential distribution, n is the outward unit normal on the boundary $\partial\Omega$, z_ℓ are the contact impedances, L is the number of electrodes, e_ℓ denotes the ℓ'th electrode and $\Omega \subset \mathbb{R}^3$ is the object. In addition, the charge conservation law

$$\sum_{\ell=1}^{L} I_\ell = 0 \tag{6}$$

must be fulfilled. Furthermore, in order to find a unique solution for the forward problem, the reference point for the potential has to be fixed. This can be done for example by setting

$$\sum_{\ell=1}^{L} U_\ell = 0\,. \tag{7}$$

The existence and uniqueness of the solution for the complete electrode model has been proven in [2].

The forward problem of EIT is to compute the potential $u = u(x)$ and the voltages U_ℓ, given the resistivity distribution ρ, the contact impedances z_ℓ and the current pattern $I = (I_1, \ldots, I_L)$. The forward problem can be approximated using the finite element method (FEM). The FEM approximation of the complete electrode model (2–7) leads to nonlinear observation model (1) where ρ is finite dimensional approximation of the resistivity with respect to chosen basis. The weak form of the complete electrode model was given in [2] and its FEM implementation in three-dimensional case in [3,4,5].

INVERSE PROBLEM IN EIT

In EIT the injected currents are known and the formed voltages are measured. The inverse problem is to determine the parameters ρ (resistivity distribution) based on the observation model (1). The inverse problem is both ill-posed and nonlinear. Due to ill-posedness of the problem, one

has to consider minimization of the (generalized) Tikhonov regularized functional

$$F(\rho) = \|V - U(\rho, z_0)\|_2^2 + \lambda^2 \|L_2(\rho - \rho^*)\|_2^2 \quad (8)$$

where V and $U(\rho, z_0)$ are the vectors consisting of the measured and computed voltages on the electrodes, respectively, λ is the regularization parameter, ρ^* is the prior for the solution and L_2 is the regularization matrix. Further, z_0 includes the contact impedances z_ℓ which are assumed to be known.

ITERATIVE RECONSTRUCTION

In this section we consider iterative minimization of the functional $F(\rho)$ in equation (8). Especially we concentrate on *line search* methods. The general form for line search methods is

$$\rho_{k+1} = \rho_k + \alpha_k p_k \quad (9)$$

where ρ_k is the k^{th} iterate, p_k is the search direction, and α_k is (a scalar) step length parameter. An example of line search methods is the *steepest descent method*

$$\rho_{k+1} = \rho_k - \alpha_k \nabla F(\rho_k) \quad (10)$$

where the search direction p_k is chosen to be the negative gradient $-\nabla F(\rho_k)$ which is known to be the direction of the steepest descent.

Usually the line search methods require computation of the gradient $\nabla F(\rho_k)$, as in the case of steepest descent method. If the functional to be minimized is of the form (8) the gradient $\nabla F(\rho_k)$ is [6]

$$\nabla F(\rho_k) = -J(\rho_k)^T b + \lambda^2 W_2(\rho_k - \rho^*) \quad (11)$$

where J denotes the Jacobian $J = \frac{\partial U}{\partial \rho}(\rho_k)$, $b = V - U(\rho_k)$, and the matrix $W_2 = L_2^T L_2$.

Computation of the Jacobian J in the case of EIT has been considered for example in thesis [6]. An advantageous procedure is to compute the Jacobian in block form, because this reduces the need of storage required for computation. Further, this method allows parallelization. Similar procedure to compute the Jacobian has been utilized also for example in optical tomography and is known as the *adjoint differentiation* [7].

In addition to choosing the step length p_k in line search (9), one also needs to choose the step length α_k. Instead of using fixed step length, it is usually preferable to use *inexact line search* [8,9,10]. In inexact line search the step length is chosen adaptively in each iteration step. The methods usually require several evaluations of the gradient ∇F corresponding to each iteration step. In practice, gradients are expensive to compute and therefore it is advisable to use less expensive methods. In some cases an effective way to choose the step parameter is to evaluate the functional $F(\rho_k + \alpha_k p_k)$ corresponding to a few different values of α_k, and fit a quadratic function to computed values.

Nonlinear Conjugate Gradient Method

The conjugate gradient method [10] is an iterative method for solving a linear system of equations

$$A\rho = c\,, \quad (12)$$

where A is $n \times n$ symmetric and positive definite matrix. The conjugate gradient method also belongs to class of line search methods, and is of the form (9). The search directions p_k are chosen to be *conjugate directions*. A set of nonzero vectors $\{p_0, p_1, p_2, ..., p_{n-1}\}$ is said to be conjugate with respect to the symmetric positive definite matrix A if

$$p_i^T A p_j = 0\,, \quad \forall i \neq j\,. \quad (13)$$

These directions are also linearly independent, and the solution for the equation (12) is found in at most n iteration steps.

The *nonlinear conjugate gradient method* (NLCG) is a line search method for minimizing nonlinear functionals F. Also in NLCG the search directions p_k are chosen to be conjugate directions; here the choice of the matrix A in (13) is based on linearization of the functional F. In NLCG the steepest descent direction is chosen to be the first search direction and the next ones are linear combinations of the steepest descent direction $-\nabla F(\rho_k)$ and the previous search direction p_{k-1}, that is,

$$p_k = -\nabla F(\rho_k) + \beta_k p_{k-1}\,. \quad (14)$$

The scalar β_k is to be determined by the requirement that p_{k-1} and p_k must be A conjugate such that $\beta_0 = 0$.

There are two algorithms for NLCG, named as the *Fletcher-Reeves algorithm* and the *Polak-Ribière algorithm* [10]. The first one is of the following form.

The Fletcher-Reeves algorithm:

Given ρ_0

Evaluate $\nabla F(\rho_0)$
Set $p_0 = -\nabla F(\rho_0)$, $k = 0$
While $\nabla F(\rho_k) \neq 0$ (or $\nabla F(\rho_k) > \epsilon$)

$$\begin{aligned} \text{Compute} \quad & \alpha_k \\ \rho_{k+1} &= \rho_k + \alpha_k p_k \\ \text{Evaluate} \quad & \nabla F(\rho_{k+1}) \\ \beta_{k+1}^{FR} &= \frac{\nabla F(\rho_{k+1})^T \nabla F(\rho_{k+1})}{\nabla F(\rho_k)^T \nabla F(\rho_k)} \\ p_{k+1} &= -\nabla F(\rho_{k+1}) + \beta_{k+1}^{FR} p_k \\ k &= k+1 \end{aligned}$$

end

We choose the step parameter α_k in each iteration step by using inexact line search as explained above. Since in the case of EIT the functional $F(\rho)$ is of the form (8), the gradient $\nabla F(\rho_k)$ is computed by using equation (11). As explained earlier, the computation can be performed economically in block form. With this choice, we refer to this method as the *block-nonlinear conjugate-gradient method*.

In Polak-Ribière method β_k is computed as

$$\beta_{k+1}^{PR} = \frac{\nabla F(x_{k+1})^T \left(\nabla F(x_{k+1}) - \nabla F(x_k)\right)}{\nabla F(x_k)^T \nabla F(x_k)} .$$

In order to assure that a new direction is descent the condition that only positive β_{k+1}^{PR} are accepted a condition

$$\beta_{k+1}^{PR} = \max\{\beta_{k+1}^{PR}, 0\} \tag{15}$$

has to be included in Polak-Ribière method. The condition (15) implies that when β_{k+1}^{PR} is negative a new search direction is chosen to be the steepest descent direction $-\nabla F(x_{k+1})$. In our numerical example we use the Polak-Ribière method, because it has been shown to be more robust and efficient than Fletcher-Reeves method, see [10].

The nonlinear conjugate gradient method assumes that the functional $F(\rho)$ quadratic. If this is not a good approximation the method may generate poor search directions. For this reason the NLCG method is sometimes improved by using *restarting* in which the search direction p_k that does not sufficiently decrease the functional F, is replaced by the steepest descent direction. There are numerous strategies for investigating if search direction is good. A typical requirement is that the angle between consecutive search directions must be large enough.

For details of nonlinear conjugate gradient method to EIT, see thesis [6]. A similar method was first applied to optical tomography in paper [11]. The method has been applied to EIT also in thesis [12] in the special case where the side constraint $\lambda^2\|L_2(\rho - \rho^*)\|_2^2$ in equation (8) is $\lambda^2\|\rho\|_2^2$ corresponding to (ordinary) Tihkonov regularization.

NUMERICAL STUDY

As a numerical test phantom a cylindrical tank with 48 electrodes, 16 electrodes in three planes was used, see Fig. 1. The radius of the tank was 15 cm and height was 20 cm.

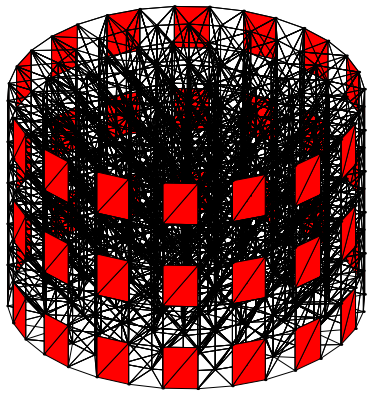

Figure 1: Geometry of the test phantom, and the FEM discretization. The rectangles on the boundary represent the electrodes.

To study the efficiency of the different reconstruction methods, the resistivity distribution shown in Fig. 2 was generated. In the sequel this distribution is referred to as *true distribution*. The simulated EIT data was computed in a mesh of 6180 tetrahedral elements and 1434 nodes, and the resistivity distribution was represented in piecewise linear basis. The tetrahedral elements formed five layers, height of each layer being 4 cm. The cut surfaces in Fig. 2 are taken from the middle of each layer. As the figure indicates, there were two inhomogeneities inside the cylinder, differing from the constant background resistivity 300 Ωcm. The resistivity of the lower inhomogeneity was 100 Ωcm in the first element layer from the bottom, increasing linearly to the background value 300 Ωcm inside the second layer. The resistivity of the upper inhomogeneity was 500 Ωcm in two uppermost element layers, decreasing linearly to the background value 300 Ωcm inside the third layer.

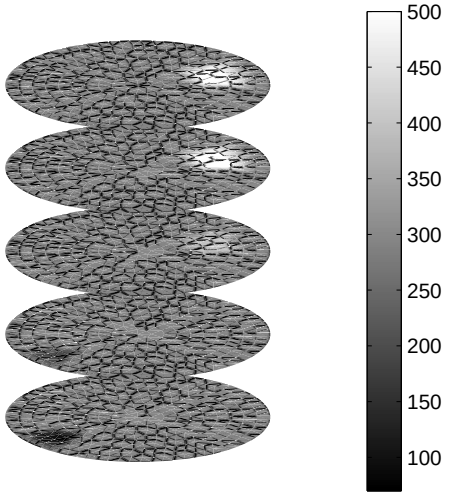

Figure 2: True resistivity distribution.

There are numerous possibilities to inject current and measure voltages in three dimensions. In this study, only in-plane current injection and voltage measurements between adjacent in-plane electrodes were used. For each current injection the voltages were measured on the remaining adjacent pairs of electrodes on each electrode plane. The voltage measurements from the current carrying electrodes were not used in the reconstructions and therefore 2160 voltage measurements were obtained. The reason for neglecting the voltages corresponding to the current carrying electrodes is that improper knowledge of the contact impedances in the real case may cause high errors in modeling those measurements [13]. Voltage observations were computed by applying the FEM to 3D complete electrode model.

Zero-mean Gaussian observation noise was added to the computed voltages. The observation noise consisted of two parts. The standard deviation (std) of the first part was 0.01% of the maximum voltage. The second part was inhomogeneous white noise, each component of the noise vector having std 1% of the value of the corresponding observation.

In the inverse computations the resistivity distribution was represented in a piecewise constant basis. The number of resistivity parameters was 2060. The initial guess for the resistivity distribution was chosen to be the best homogeneous estimate, see [14]. As the regularization matrix L_2 we used a difference matrix corresponding to *smoothness prior*. The regularization parameter λ was chosen by visual inspection, because the traditional methods for choosing the regularization parameter are not suitable in the case of EIT. It is worth to notice, however, that in the real case the use of visual examination is not possible, since the true resistivity distribution is unknown. The question of choosing the regularization parameters in different types of inverse problems is a topic of on-going research. The aim of this study is not to consider this topic. Instead, the aim is to compare the efficiency and computational storage of different optimization methods applied to minimization problems with predetermined priors.

The Figure 3 represents the NLCG-estimate for the resistivity distribution after 260 iterations steps.

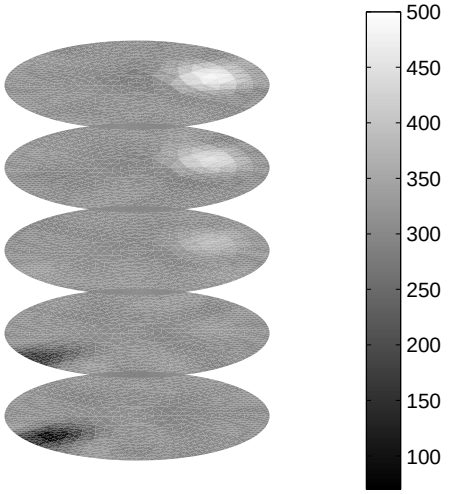

Figure 3: Conjugate gradient reconstruction after 260 iteration steps..

The two inhomogeneities inside the object are well located. In addition, the absolute values of the inhomogeneities are recovered relatively well. This is also shown in Figure 4, which represents the maximum and minimum values of the reconstructed resistivity distributions in each iteration step.

For comparison, we also computed the estimates by using the steepest descent method (10) and the Gauss-Newton method. In the case of functional (8) the Gauss-Newton iteration gets the form

$$\rho_{k+1} = \rho_k + \alpha_k \left(J(\rho_k)^T J(\rho_k) + \lambda^2 W_2 \right)^{-1} \cdot (J(\rho_k)^T (V - U(\rho_k)) - \lambda^2 W_2 (\rho_k - \rho^*)), \quad (16)$$

see for example [6]. All the methods converged to the same solution, since the same functional (8)

was minimized in all methods. However, there were differences in the convergence rates, computation times and in the computer storage needs.

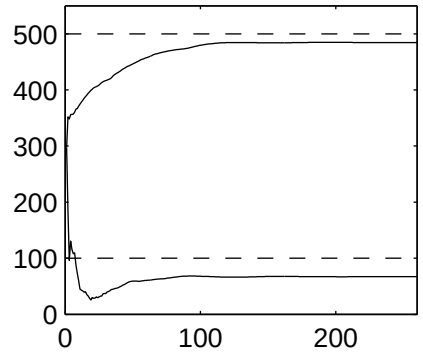

Figure 4: Convergences of the maximum and minimum resistivity values of the reconstructions during the iterations in NLCG. The dashed lines mark the true minimum and maximum values.

The convergence of the Gauss-Newton method was superior to NLCG and steepest descent method. The maximum and minimum values of the Gauss-Newton iterates are represented in Figure 5. The algorithm is practically converged already after three iteration steps.

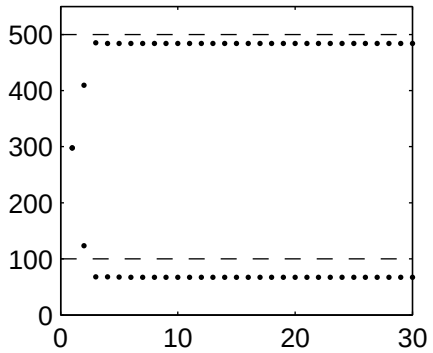

Figure 5: Convergences of the maximum and minimum resistivity values of the reconstructions during the iterations in Gauss-Newton method. The dashed lines mark the true minimum and maximum values.

Figure 6 represents the convergence rates of the three different optimization methods. As noted above, the Gauss-Newton method converges most rapidly. Further, the convergence rate of steepest descent is seen to be far slower than the convergence rate of the NLCG method.

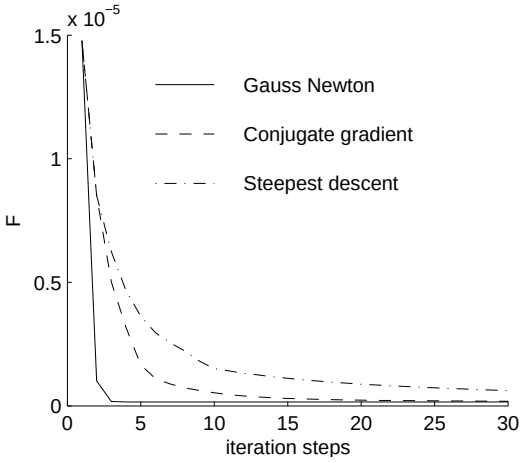

Figure 6: Comparison of the convergence rates. Value of the functional $F(\rho)$ in first 30 iteration steps for different optimization methods.

The differences in the convergence rates are indicated also in Table 1. The listed numbers of iteration steps are the numbers of iterations required for reducing the value of the functional $F(\rho_k)$ below a certain predetermined level. The NLCG method with restarting is also listed in the table. As the figures indicate, the use of restarting does not have a considerable effect in our example case. Table 1 also shows the computer storage needs in cases of different optimization methods. The drawback of the Gauss-Newton method is that it requires more storage than the other methods. This is due to matrix inversion required in each iteration step (16). The NLCG method does not require much more storage than the steepest descent method, but the convergence rate is much better than in the case of steepest descent method.

Table1: Comparison of different optimization methods. The memory need is expressed in Megabytes.

Method	Iterations	Memory need
Gauss-Newton	10	41.3230
NLCG	260	8.1984
- restarting	247	8.1984
Steepest descent	4 000	8.1654

Finally we studied the effect of inexact line search in NLCG method. Figure 7 shows the convergence of the iteration with inexact line search and with two fixed step parameters α_k. Inexact line search has a remarkable impact on conver-

gence rate. Further, the figure indicates that the optimal values of the step parameter are far from the standard choice $\alpha_k = 1$.

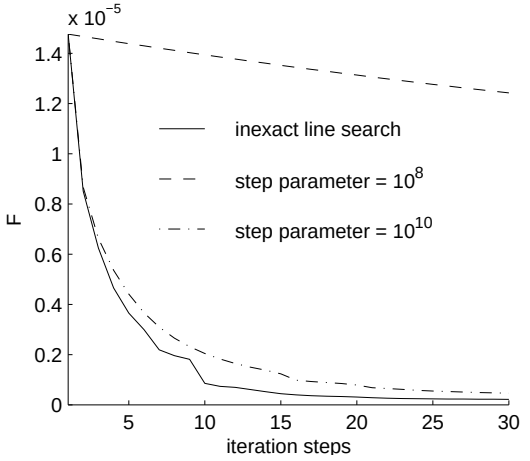

Figure 7: Convergence of the NLCG iteration with inexact line search and with two fixed step parameters.

The effect of inexact line search was also tested in cases of steepest descent and Gauss-Newton method. As in the case of NLCG method, in steepest descent method the inexact line search improved the performance of the algorithm remarkably, where as in Gauss-Newton method it did not have a significant effect on the convergence rate.

CONCLUSIONS

In this paper we studied iterative methods in EIT. We proposed a novel block-nonlinear conjugate-gradient method for EIT, and compared it with traditional methods using a numerical simulation.

Three-dimensional imaging in EIT, especially in cases of complex geometries, leads to large dimensional systems of equations, and the choice of optimization method plays a significant role. The features that one should consider when choosing the optimization method are: 1) convergence rate, 2) computation time, and 3) need of computer storage. The convergence rate of Gauss-Newton method was noticed to be superior to other methods. However, the Gauss-Newton iteration also requires considerably more computer storage than for example steepest descent method. The drawback of steepest descent method is the slow convergence.

The proposed block-nonlinear conjugate-gradient method was shown to converge much more rapidly than the steepest descent method. In addition, the need of storage is of the same order than in the case of steepest descent method. These features make the proposed method tempting in the case of large dimensional problems.

The comparison of computation times is a bit problematic, because the ratios of computation times depend on the dimension of the problem, and the capacities of the computer. In our example case the geometry of the domain was simple, and the number of unknowns was relatively small, 2060. For this reason, in our case the computation time was shortest for the Gauss-Newton method. However, when the number of unknowns gets larger the Gauss-Newton method gets slower in comparison with the NLCG method, and finally when the storage limit of the computer is exceeded, the method becomes completely inapplicable.

REFERENCES

1. K.-S. Cheng, D. Isaacson, J.C. Newell, and D.G. Gisser. Electrode models for electric current computed tomography. *IEEE Trans Biomed Eng*, **36**, 918 (1989)

2. E. Somersalo, M. Cheney, and D. Isaacson. Existence and uniqueness for electrode models for electric current computed tomography. *SIAM J. Appl. Math.*, **52**, 1023 (1992)

3. P.J. Vauhkonen, M. Vauhkonen, T. Savolainen, and J.P. Kaipio. Three-dimensional electrical impedance tomography based on the complete electrode model. *IEEE Trans. Biomed. Eng.*, **46**, 1150 (1999)

4. P.J. Vauhkonen, M. Vauhkonen, T. Savolainen, and J.P. Kaipio. Static three-dimensional electrical impedance tomography. *Ann New York Acad Sci*, **873**, 472 (1999)

5. P.J. Vauhkonen. Second order and infinite elements in three dimensional electrical impedance tomography. Phil. Lic. thesis, University of Kuopio, Finland, 1999

6. P.J. Vauhkonen. *Image Reconstruction in Three-Dimensional Electrical Impedance Tomography*. PhD thesis, University of Kuopio, Kuopio, Finland, 2004

7. S. R. Arridge. Optical tomography in medical imaging. *Inv Probl*, **15**, R41 (1999)

8. R. Fletcher. *Practical methods of optimization*. John Wiley & Sons Ltd., 1987

9. P.E. Gill, W. Murray, and M.H. Wright. *Practical optimization*. Agademic Press, Inc., 1981

10. J. Nocedal and S.J. Wright. *Numerical optimization*. Springer series in operations reseach. Springer-Verlag, New York, 1999

11. S. R. Arridge and M. Schweiger. A general framework for iterative reconstruction algorithms in optical tomography, using a finite element method. In C. Borgers and F. Natterer, editors, *Computational Radiology and Imaging: Therapy and Diagnosis*, volume 110 of *IMA Volumes in Mathematics and its Applications*, pages 45–70. IMA, Springer-Verlag, 1998

12. N. Polydorides. *Image reconstruction algorithms for soft-field tomography*. PhD thesis, UMIST, 2002

13. L.M. Heikkinen, T. Vilhunen, R.M. West, and M. Vauhkonen. Simultaneous reconstruction of electrode contact impedances and internal electrical properties: II. Laboratory experiments. *Measur Sci Technol*, **13**, 1855 (2002)

14. S. Järvenpää. A finite element model for the inverse conductivity problem. Phil. Lic. thesis, University of Helsinki, Finland, 1996